# The Role of ENSO in the South Asian Monsoon and Pre-Monsoon Signals Over the Tibetan Plateau

**K. MIYAKODA, J.L. KINTER III**

*Center for Ocean-Land-Atmosphere Studies, Maryland, USA*

**and**

**Song YANG**

*Climate Prediction Center, National Weather Service, National Oceanic and Atmospheric Administration, Maryland, USA*

*(Manuscript received 5 March 2002, in revised form 5 June 2003)*

## Abstract

El Niño and the Southern Oscillation (ENSO), and the South Asian (SA) summer monsoon interact with each other. In a previous paper, the process from the SA-monsoon to ENSO was discussed. In this paper, the process from ENSO to the monsoon is described.

As the consequence of ENSO events, a set of characteristic distributions of the temperature, wind and moisture is formed over the central and eastern Pacific Ocean. The anomalies of these fields are characterized by a "butterfly pattern" above the 500 hPa level, and a "horseshoe pattern" below 500 hPa. The patterns begin to appear in the winter, and influence the SA-monsoon in the following spring and summer. The distinct pattern of the butterfly shape may be explained by the extended Matsuno-Gill type dynamics, because the Pacific sector is dominated by the ENSO heating.

On the other hand, the Indian sector is characterized by the land-sea monsoon circulation. It is important to note that the anomaly components of this local circulation are controlled largely by ENSO. The air temperature anomaly of the layer between 200 and 500 hPa moves westward in the latitude belt of 20°–35°N over the Asian sector, which is associated with the butterfly pattern in the Pacific sector. During this migration, the signal provides a precursory background over the Tibetan Plateau in April-May-June at its peak, setting the stage for the initiation of the SA-monsoon. Another signal emanates also from the tropical Pacific to the Indian sector, in May-June-July at its peak, in conjunction with the horseshoe pattern of the sea surface temperature in particular. These signals emanate from the eastern part of the ENSO region, contribute to the establishment of the thermal contrast anomalies between land and ocean, and the anomalous wind system over the Indian sector, including the upward motion over the Indian subcontinent. The EOF (empirical orthogonal function) analysis of the sea surface temperature in the broader NINO3 region (15°N–15°S, 150°W–90°W) indicates that the two leading modes well represent the fields of horizontal wind and temperature for the Pacific sector (the first mode) as well as the Indian sector (the second mode).

Finally, the features associated with the 1976 climate shift are discussed. In the process from the SA-monsoon to ENSO, the mode of connection changed dramatically circa 1976; however, in the process from ENSO to the monsoon, the mode is almost the same before and after 1976. The reason for this asymmetry, in the change of the relationship, is discussed.

Corresponding author: Kikuro Miyakoda, 608 Sayre Drive, Princeton, NJ 08540, USA.
E-mail: miyakoda@juno.com

## 1. Introduction

There are at least three factors that are responsible for the annual occurrence of the South Asian (SA) summer monsoon. One is the land-sea thermal contrast between the South Asian land mass and the Indian Ocean, which is established prior to the monsoon season. Another is the influence of the Tibetan Plateau (e.g., Staff Members of Academia Sinica 1957; Flohn 1957; Hahn and Manabe 1975; Luo and Yanai 1984; He et al. 1987; Yanai et al. 1992; Wu and Zhang 1998). Although these factors set up the background of the monsoon, interannual variations of the monsoon are also affected significantly by a third factor, i.e., El Niño and the Southern Oscillation (ENSO; e.g., Angel 1981; Rasmusson and Carpenter 1983; Shukla and Paolino 1983; Webster and Yang 1992; Palmer et al. 1992; Webster et al. 1998). For this reason, the SA-monsoon may also be viewed as a part of a tropical-wide zonal oscillation (Navarra et al. 1999; Miyakoda et al. 1999).

In addition to these three factors, a fourth element affecting the interannual variability of the monsoon has been mentioned often, namely, the Indian Ocean sea surface temperature (SST; for example, Shukla 1975; Washington et al. 1977; Yamazaki 1988; Chandrasekar and Kitoh 1988; and Meehl and Arblaster 2002a). However, as will be discussed in section 5, two classes of argument continue. One argument is that the interannual variability of the SA-monsoon can be produced without SST anomalies is the Indian Ocean due to the remote effect of ENSO. The other argument is that the effect of the Indian Ocean dipole mode (Saji et al. 1999) may have a serious impact on the monsoon rainfall over the Indian subcontinent.

Among the elements described above, the present paper focuses primarily on the external effect, i.e., the effect of ENSO on the SA-monsoon. Recently, Kawamura (1998) presented evidence of a precursory signal for the SA-monsoon, which moves from the North Pacific to the Tibetan Plateau. Liu and Yanai (2001) depicted this signal by examining the statistical relationship between Indian monsoon rainfall, and the large-scale tropospheric and stratospheric temperature over the Eurasian continent.

In previous studies by Miyakoda et al. (2000), and Kinter et al. (2002), the processes from the SA-monsoon to ENSO were discussed. One of their conclusions is that the sequence changed circa 1976. The shift occurred in association with the change in the surface wind over the North Pacific, and the eastern seaboard of Asia. For example, the correlation coefficient between the Indian monsoon rainfall, and subsequent NINO3 SST, is $-0.74$ before 1976, while it is only $-0.25$ after 1976 (see Table 4 of Kinter et al. 2002).

The processes from ENSO to the SA-monsoon have been investigated in a number of studies, for example, Ropelewski and Halpert (1989), Webster and Yang (1992), Brankovic et al. (1994), Ju and Slingo (1995), Shen and Lau (1995), Arpe et al. (1998) and Wang et al. (2000), among others. The objectives of this paper are to explore another comprehensive description of the signals over the Tibetan Plateau and the Pacific, to understand the role of ENSO, to display the relationship of the monsoon with the signals from the eastern Pacific Ocean sector, and to investigate the long-term variability of the ENSO-to-monsoon convection.

## 2. Data and indices

This study uses the monthly mean data from the National Centers for Environmental Prediction and the National Center for Atmospheric Research (NCEP/NCAR) reanalysis (Kalnay and coauthors 1996) for the period 1955–97. It also uses the SST data produced by Reynolds and Smith (1994).

In the analysis, four major indices are employed. They are the NINO3 SST index (5°N–5°S, 150°W–90°W) taken from the NCEP website (http://www.cpc.ncep.noaa.gov), the All-India monsoon Rainfall (AIR), the Webster-Yang monsoon index (W-Y), and the meridional thermal gradient (MTG) index. The AIR (see Mooley and Parthasarathy 1983) is the rainfall averaged over India for the months from June to September (JJAS). The W-Y index was derived by Webster and Yang (1992), for representing the dynamical aspects of the Asian monsoon. It is defined by the vertical difference of the area-averaged zonal winds between 850 and 300 hPa (i.e., $\text{W-Y} = U_{850} - U_{200}$) over the region (0°–20°N, 40°–110°E). This index has been used widely in monsoon research (e.g., Ju

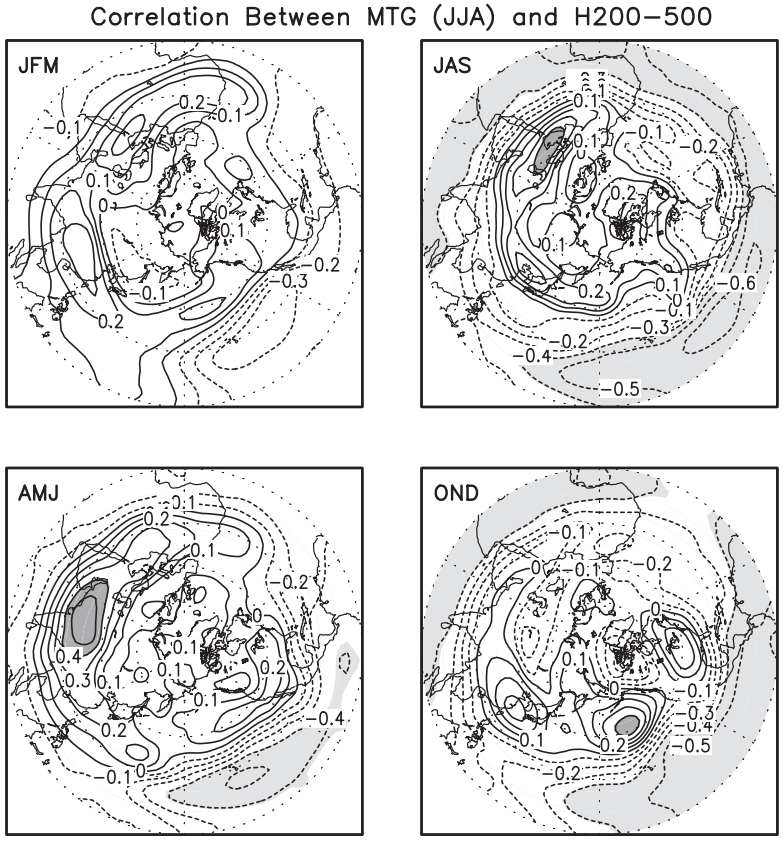


Fig. 1. Correlation between the host index MTG and the grid-point thickness (H200–500) of the various seasons (JFM, AMJ, JAS, and OND) for the period of 1955–97. Absolute values larger than 0.39 are shaded.

and Slingo 1995; Yang et al. 1996; Yang and Lau 1998; Goswami et al. 1999; Lau et al. 2000; Wang et al. 2000; Liu and Yanai 2001; Kinter et al. 2002). The MTG index was proposed by Kawamura (1998), measuring the meridional difference in area-averaged 200–500 hPa thickness ($H_{200}$–$H_{500}$) between two regions: the northern Indian Ocean (0°–20°N, 50°–100°E), and the Tibetan Plateau (20°–40°N, 50°–100°E). That is, $\mathrm{MTG} = (H_{200-500})_{(20-40\,\mathrm{N})} - (H_{200-500})_{(0-20\,\mathrm{N})}$. In spite of the difference in spatial domain and vertical level, MTG should be similar to W-Y insofar as the geostrophic approximation applies.

Among the main indices described above, the June-July-August (JJA) mean values are used for W-Y and MTG, and the JJAS means of rainfall are used for AIR. It is known that AIR does not include the rainfall over the entire South Asian region (see Fig. 2 of Miyakoda et al. 2000). For example, the rainfall over the Bay of Bengal is entirely missing from AIR. For this reason, MHI (the Monsoon Hadley Circulation Index) was proposed by Goswami et al. (1999), which is also used as a complementary index in this study.

## 3. Signals passing through the Tibetan Plateau

Kawamura (1998) points out the outstanding pre-monsoon signals that exist off Alaska (about 45°N), which are in some way associated with other signals over the Tibetan Plateau. This signal is particularly evident in the thickness between 200 and 500 hPa. The atmospheric circulation is counter-clockwise (clockwise) for weak (strong) monsoon cases. Liu and Yanai (2001) also show the high correlation between the temperature at various levels and

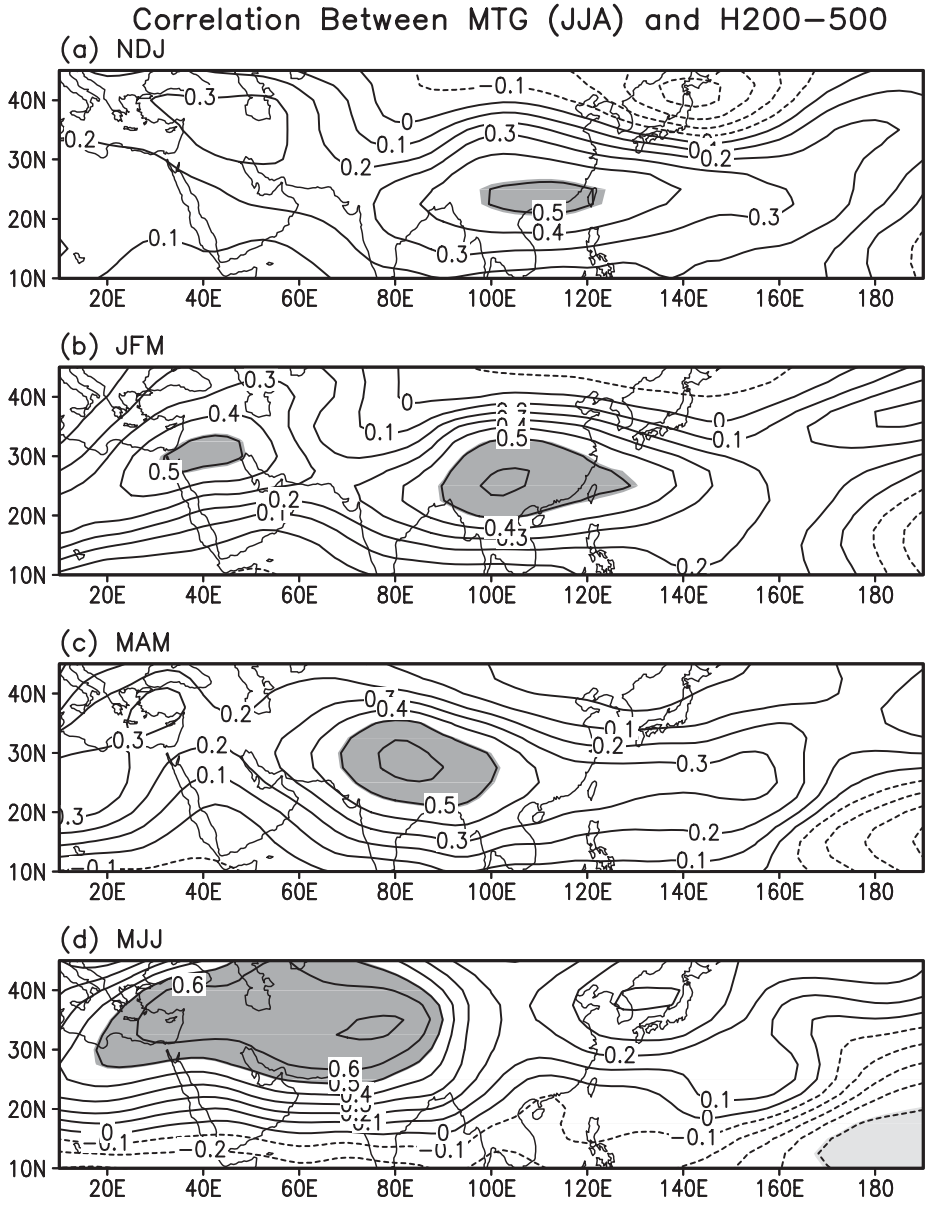


Fig. 2. Correlation between the host index MTG and the grid-point thickness (H200–500) of the various seasons (NDJ, JFM, MAM, and MJJ) before the South Asian summer monsoon. Values significant at 99.9% confidence level are shaded.

the monsoon index, such as AIR or W-Y. According to their study, the high correlation levels are found between 200 and 600 hPa for MAM and JJAS.

Figure 1 shows the patterns of correlation between MTG and the $H_{200-500}$ for different seasons. In the figure, JFM, AMJ, JAS, and OND stand for January-March, April-June, July-September, and October-December, respectively. In this figure, a high correlation area is defined as an area where the correlation is $>0.39$, significant at the 99% confidence level. High correlation areas appear over the equatorial region as well as the latitudes 20°–35°N. A particular example is the subtropical band that extends from the Pacific to Morocco, close to the Atlantic Ocean. It should also be stressed that the correlation is particularly

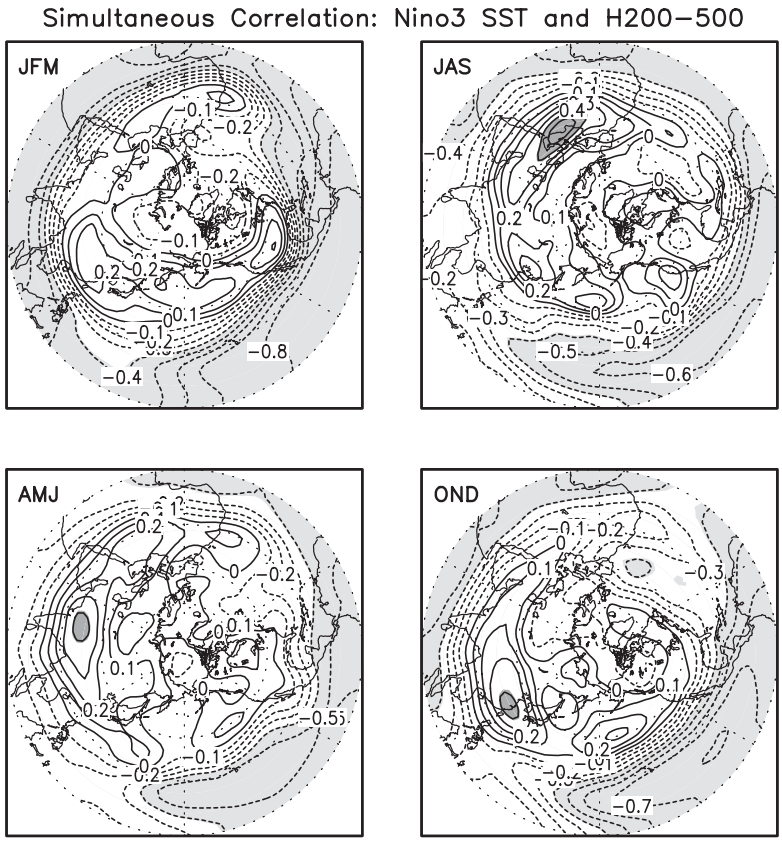


Fig. 3. Simultaneous correlation between −[NINO3 SST] and grid-point thickness (H200–500) for JFM, AMJ, JAS, and OND. Absolute values larger than 0.39 are shaded.

strong over the Tibetan Plateau, as seen in AMJ.

To make a better examination of the detailed features over the Tibetan Plateau, we plot in Fig. 2 the time sequence of the horizontal maps from NDJ (November-January) to MJJ (May-July), prior to the SA-summer monsoon. The figure shows the seasonal evolution of the high correlation areas between MTG (JJA) and $H_{200-500}$. The correlation within the shaded areas is significant at the 99.9% confidence level. The most striking features are the following. (1) The high correlation area appears first in the east, and moves steadily toward the west. (2) The high correlation area over India is in a "lens" shape. (3) There are two maxima: one at 100°E, and the other at 40°E in the JFM panel. It should be noted that the climatological mean westerlies at 200 hPa are very weak, or become easterlies over these areas (not shown).

Changing the host index from MTG to NINO3 SST, the simultaneous correlation between NINO3 SST and $-H_{200-500}$ for the various seasons is calculated (Fig. 3). Not surprisingly, the strongest correlation is usually found over the equatorial Pacific. However, our interest is over India. Another maximum with the opposite sign is found there in AMJ. The high positive correlation area extends nearly to Europe in JAS, and then decays in OND. This result is consistent with that of Wang et al. (2000), who described the movement of the area as "emanation", instead of propagation.

The global horizontal emanation of the high correlation area changes slightly when different indices are used, so far as the patterns at 20°–35°N are concerned. For example, the maximum correlation between the $H_{200-500}$ of AMJ, and various indices, is 0.68 for MTG, −0.52 for NINO3 SST (JAS), 0.52 for W-Y, and 0.41 for AIR. All of these maxima are found over the Tibetan Plateau.

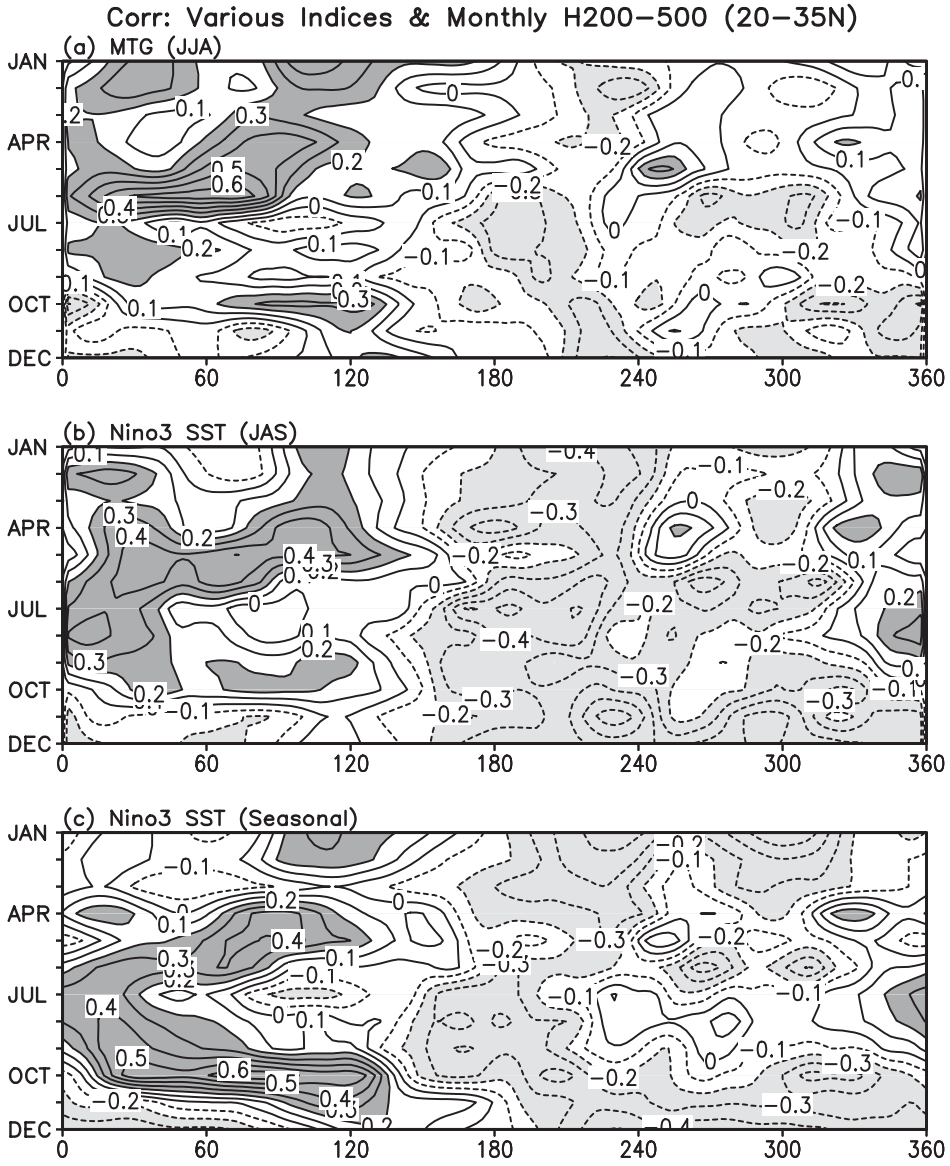


Fig. 4. (a) Time-longitude section of the correlation between MTG and the monthly thickness (H200–500) of the latitude belt of 200 N–350 N. (b) Same as in (a), but MTG is replaced by −[NINO3 SST] (JAS). (c) Same as in (a), but MTG is replaced by the seasonal means of −[NINO3 SST] in JFM, AMJ, JAS, and OND (representing the near-simultaneous correlation between the SST and the thickness). Absolute values larger than 0.2 are shaded.

The time-longitude sections related to these results are shown in Fig. 4, which presents the correlation between the $H_{200-500}$ averaged over 20°–35°N and MTG. In this figure, the seasonal means of NINO3 SST for JFM, AMJ, JAS, and OND are used as the host indices, while the target variables are January, February and March separately for the first three months, and then April, May, June, separately, for the second three months, etc. Therefore, the host index and the target variable in the correlation are nearly simultaneous.

Figure 4 suggests that the positive high correlation areas appear at 120°E in January. However, according to an extended analysis starting from OND in the previous year (not

Table 1. Correlation between three monsoon indices (left column) and the H200–500 and T300 averaged over the Himalayas and western Eurasia. The italic bold numbers are above 99.9% confidence level, and the bold numbers are between the 99.9% and 90.0% levels.

| | H200–500 (MAM) | | T300 (MAM) | |
|---|---|---|---|---|
| | Himalayas | W. Eurasia | Himalayas | W. Eurasia |
| AIR (JJAS) | **0.45** | **0.44** | **0.42** | **0.4** |
| W-Y (JJA) | ***0.56*** | ***0.49*** | ***0.56*** | **0.45** |
| MTG (JJA) | ***0.58*** | 0.36 | ***0.57*** | 0.33 |

shown), instead of NDJ (as in Fig. 2), the high correlation region appears in OND at a higher latitude near 43°N in the western hemisphere (140°W) (not shown here, but can be speculated from Kawamura 1998). In agreement with the result of Liu and Yanai (2001), Fig. 4 shows that, in the earlier half of the year, the signal moves westward from the mid-Pacific to the prime meridian (North Africa). However, in the later half of the year, the strong positive correlation area moves eastward. The movement looks like a "boomerang". This is one of the highlights of this particular teleconnection. The high negative correlation area at 180°–240°W is the northward expanding area of ENSO effect (see Figs. 3 and 1).

How can this boomerang-shaped movement be explained? It is speculated that this displacement is associated with the seasonal change of the geopotential height pattern in the layer between 500 and 200 hPa level. The monthly mean wind field at 200 hPa level, for example, is characterized by a large anticyclonic flow with its center at 85°E and 25°–30°N (see Fig. 2 of Li and Yanai 1996). This center moves gradually first westward, and then reverses after July. The view of the seasonal migration, as opposed to a dynamical propagation, is supported by the fact that a similar, but weaker correlation area, appears in the Southern Hemisphere (see Liu and Yanai 2001). Moreover, this phenomenon is only evident over land, not over ocean (see later Figs. 8 and 9). Based on these facts, it speculated that this is, after all, the seasonal movement of the heated area mostly over the Asian continent, but to a lesser extent over the Australian, and South African continents.

## 4. Characteristics of signal over the Pacific and the Indian sectors

### *4.1 Property of the signal over the Tibetan Plateau*

The importance of the Tibetan Plateau for the SA-monsoon is discussed by comparing the features over the Himalayas and western Eurasia. Table 1 shows the lag correlation between the monsoon indices (AIR, W-Y, and MTG), the MAM $H_{200-500}$ and $T_{300}$ over the Himalayas (20°–35°N, 60°–100°E; see Fig. 5), and over western Eurasia (20°–40°N, 10°–80°E). First, this table shows that the values of correlation are similar for $H_{200-500}$ (left) and $T_{300}$ (right). Second, the signal over the Himalayas is considerably stronger than that over western Eurasia. Therefore, the Tibetan Plateau is more appropriate than western Eurasia as the location of the pre-monsoon signal. On the other hand, Kawamura (1998) shows that the April-May $T_{850}$ west of the Himalayas (25°–40°N, 50°–80°E) is most strongly related to the AIR. Later, Kawamura et al. (2001) re-emphasized that the downdraft is dominant in this region before the start of the monsoon.

In order to examine how the $H_{200-500}$ over the Tibetan Plateau is related to the SA-monsoon, the seasonal variations of the correlation between the $H_{200-500}$ index (20°–35°N, 60°–100°E; see the shaded area in Fig. 5) and the different monsoon indices (JJA or JJAS) are analyzed. It is seen from Fig. 6 that the strongest correlation appears in AMJ for MTG and W-Y, and in MAM for AIR. The value of correlation decreases in the order of MTG, W-Y, and AIR. The correlation is overall not very strong, suggesting that the Himalayas signal is

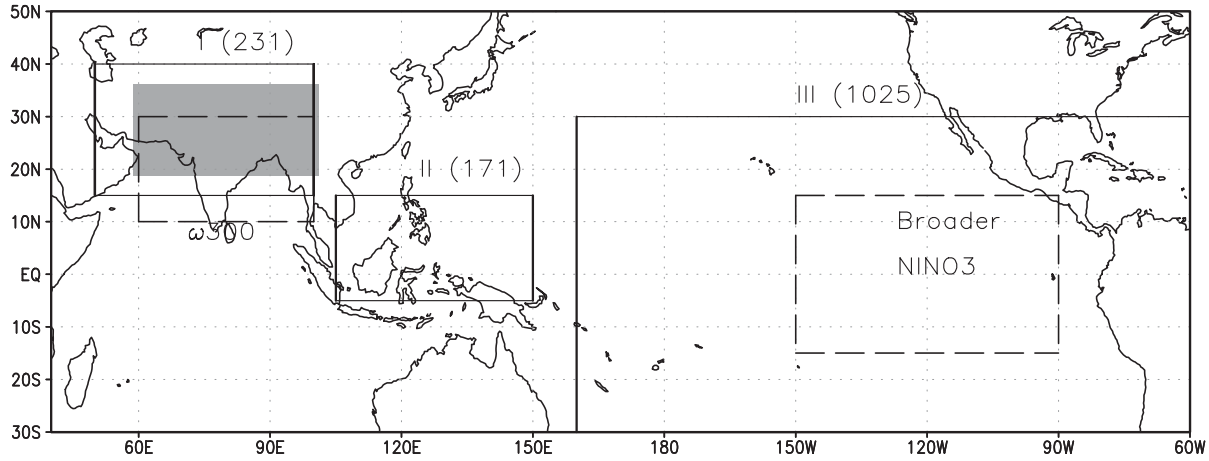


Fig. 5. The three domains that are the foci of this study, especially in Table 2. The number in the parentheses of each domain is the number of total grid-points of reanalysis data inside that domain. The shaded area is the Tibetan Plateau (Himalayas), in which the pre-monsoon signal of H200–500 is defined. The area of w 300 for the EOF analysis (small dashed area) is indicated. The small dashed-line box within Domain III is the "broader NINO3", whose SST is used for EOF analysis.

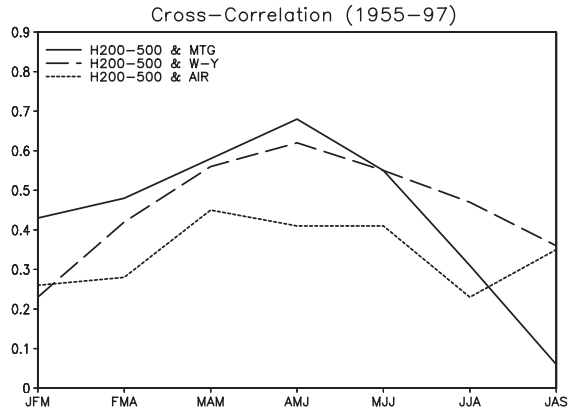


Fig. 6. Display of the correlation between the thickness (H200–500) index over the Tibetan Plateau and three summer monsoon indices (AIR, W-Y, and MTG) as a function of time. The seasons shown in the abscissa are for the thickness.

not the full explanation for triggering the monsoon. The land-sea contrast between the Indian Ocean and the Indian subcontinent is certainly another important factor. The significance of the precursory signal over the Tibetan Plateau toward the southeast Asian monsoon is summarized by Li and Yanai (1996), for example. The contribution of the Tibetan Plateau to the SA-summer monsoon is unique, and the intensity of rainfall is large. For these reasons, this monsoon is ranked as one of the most dominant and influential climate phenomena.

The vertical velocity is one of the important indicators of the SA-monsoon. We have made a preliminary analysis to determine that the most appropriate level for representing the vertical velocity associated with the monsoon is 300 hPa (see also Lau et al. 2000, and Miyakoda et al. 2000). Yet we notice that it is inappropriate to calculate the simple area average of the vertical motion at 300 hPa ($\omega$300) over the monsoon region, because it has two major centers in April-May, one over the Bay of Bengal and the other over the region of northeast Africa and southwest Asia. Besides, it is quite irregular in space. For this reason, the empirical orthogonal function (EOF) analysis is used to characterize the variability of vertical velocity in the SA region. The EOFs of $\omega$300 anomalies are calculated for two different domains to test the sensitivity of the result. One is an area covering 60°–100°E, 10°–30°N, labeled $\omega$300 in Fig. 5. The other is a larger area covering 50°–100°E, 10°–40°N (not shown).

Figure 7 presents the correlation between monsoon indices (JJA or JJAS) and the first

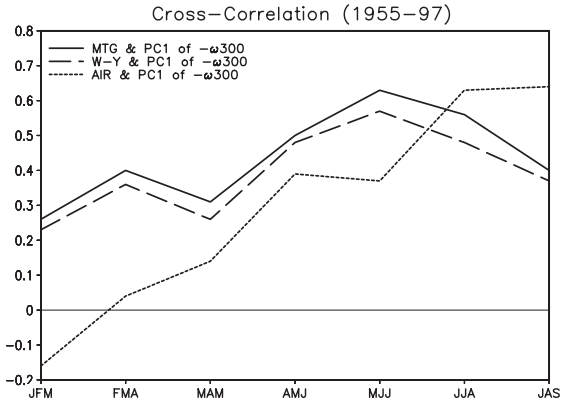


Fig. 7. Same as in Fig. 6, but the values of the time-varying thickness are replaced by those of the first principal component of $-\omega 300$.

principal component (PC1) of $\omega 300$ over the smaller area for various seasons. The figure indicates that the correlation with the monsoon updraft reaches the 99.0% confidence level in AMJ. However, the maximum is somewhat different for MTG and W-Y compared to AIR, because AIR is based on the precipitation, and it depends not only $\omega 300$ but also on the moisture supply (see for example, Shen and Kimoto 1999). It is generally known that the monsoon peak is JJAS or JAS. The curve of AIR reflects this fact most faithfully, while the curves of MTG and W-Y do not. The correlation is also dependent on the size of the EOF analysis area. For example, the maximum occurs in MJJ for the smaller area (Fig. 7), but in AMJ for the larger domain (not shown).

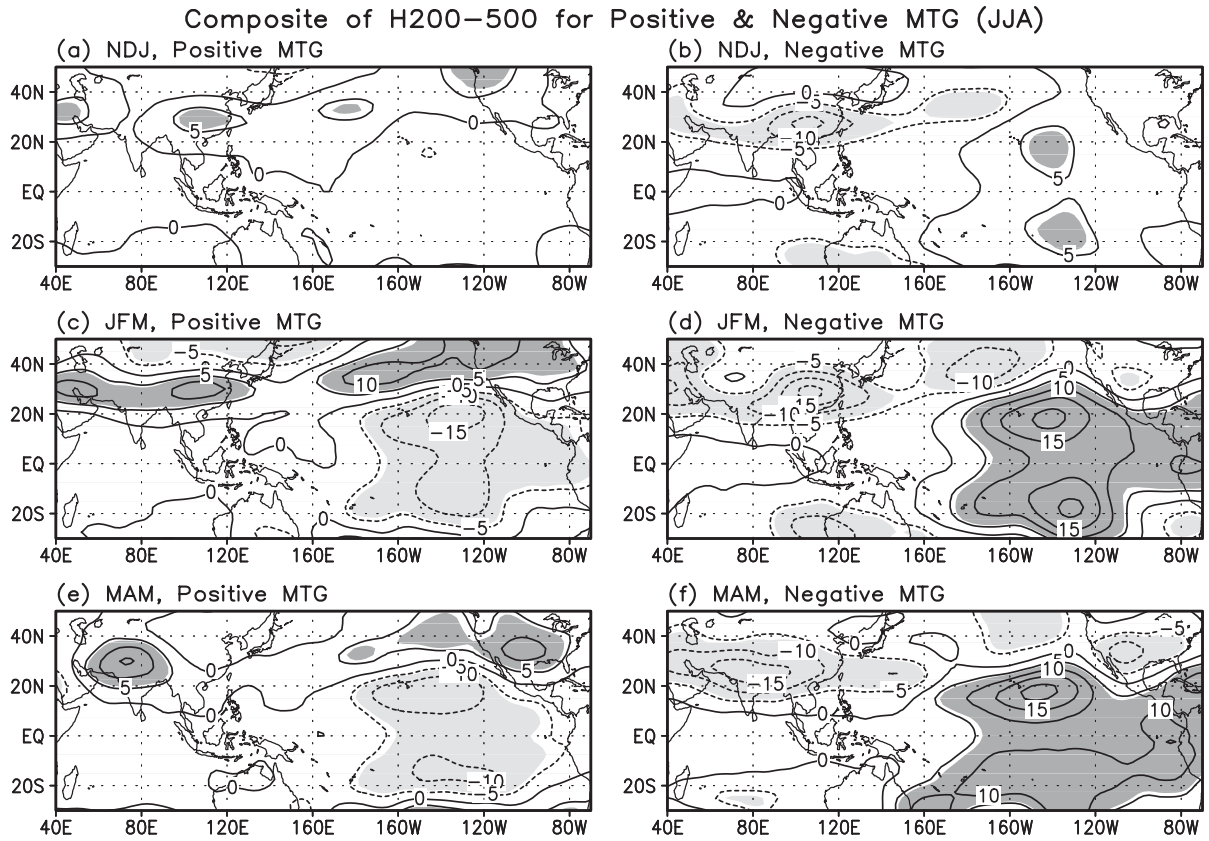


Fig. 8. Composite patterns of the H200–500 anomalies for strong and weak monsoons measured respectively by positive and negative MTG. Strong cases are 1961, 67, 71, 75, 78, 81, 84, 85, 90, and 94. Weak cases include 1956, 57, 69, 72, 76, 77, 83, 87, 92, and 97. The diagrams are constructed for the NDJ (a and b), JFM (c and d), and MAM (e and f) before the monsoon. Units are in meters. Absolute values larger than 6 meters are shaded.

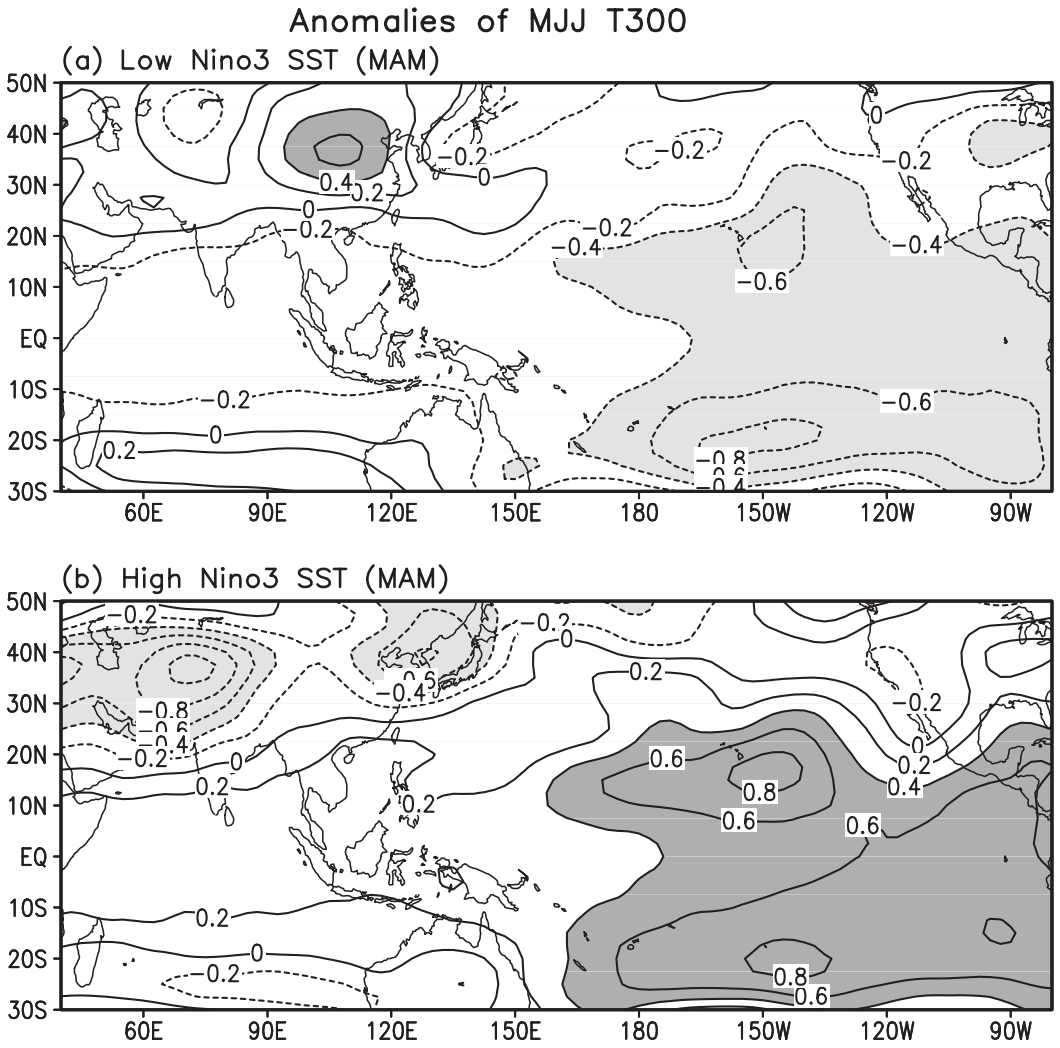


Fig. 9. Composite patterns of the MJJ T300 anomalies for La Niña (a) and El Niño (b) cases selected by MAM NINO3 SST. El Niño cases include 1957, 58, 69, 72, 82, 83, 87, 92, and 97. La Niña cases are 1955, 62, 64, 67, 68, 71, 75, 85, 88, and 89. Absolute values larger than 0.4 are shaded.

### *4.2 Characteristics of the signal over the tropical Pacific Ocean*

Figure 8 shows the composite patterns of H200–500 anomalies for NDJ, JFM, and MAM. The figure is constructed based on the ten largest positive and ten largest negative cases of MTG (JJA). In general, the highly anomalous centers correspond well to the high correlation areas shown in Fig. 2, and are similar to the features in the composite patterns of 200 hPa stream function shown by Kawamura et al. (2001). It is characteristic that the patterns in Fig. 8 are almost anti-symmetric between the left and right panels. The symptom of this systematic demarcation can be detected in NDJ, but not very clearly (Figs. 8a and 8b). It becomes much clearer in JFM (Figs. 8c and 8d), and it remains the same in MAM (Figs. 8e and 8f).

Figures 9 and 10 are the composites of T300 and T850 anomalies for MJJ, which are constructed based on the warm and cold cases based on the sign and the magnitude of NINO3 SST of MAM. These figures illustrate that the patterns over the Pacific are divided into two types. The pattern of T300 is of a butterfly

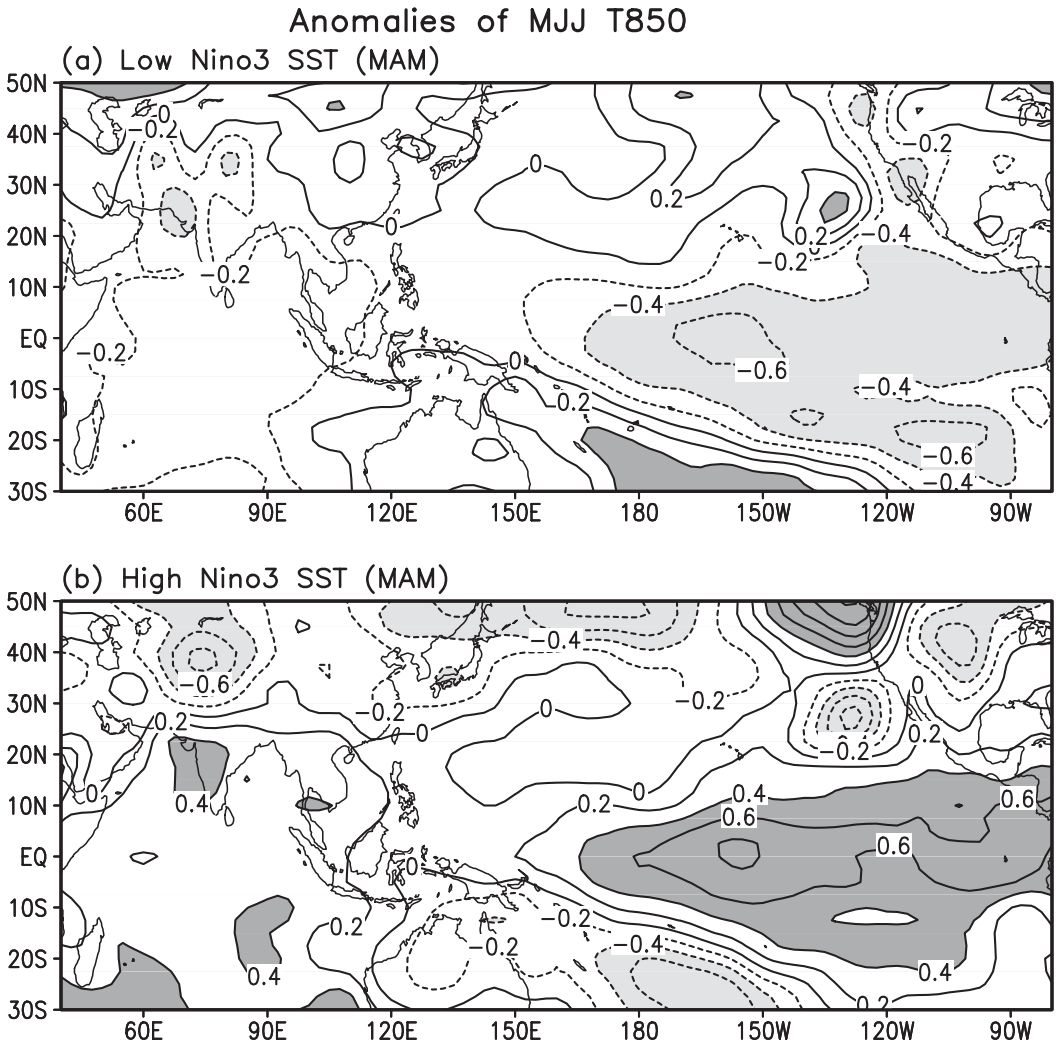


Fig. 10. Same as in Fig. 9 except for the T850 anomalies.

shape, while that of T850 is of a horseshoe shape. The butterfly pattern is found in the higher troposphere (in T200 and T300), while the horseshoe pattern is found in the lower troposphere (in T700 and T850). T500 is characterized by a mixture of the features in the upper and lower troposphere (see also Table 2). This result is consistent with that of Wang et al. (2000), as shown in their Fig. 6.

The butterfly pattern over the Pacific sector is essentially the Matsuno-Gill type response to the tropical heat source (Matsuno 1966; and Gill 1980; see Kawamura 1998). In the original study of Gill, positive heat sources of a short longitudinal length are set up at the Equator. As a result, Hadley cells are produced in both hemispheres symmetrically, which corresponds to the butterfly pattern.

Using "perturbation models" or "anomaly models", instead of General Circulation Models (GCMs), the effects of ENSO heating over the Pacific region were studied by Nigam et al. (1986; 1988), Navarra and Miyakoda (1988), and Ting and Held (1990). All these papers compare their solutions with those of GCMs for the case of dipole heating. El Niño, for example, generates positive heating anomalies over the equatorial zone, associated with strong upward circulation anomalies throughout the troposphere. With these upward motion anomalies,

Table 2. Spatial correlation coefficients (CC) of the temperature anomalies (MJJ) between El Niño and La Niña cases. See Fig. 5 for details of the three domains: I, II, and III. The absolute values of CC larger than 0.70 are bold.

| | I | II | III | I | II | III |
|---|---|---|---|---|---|---|
| | T200 (Butterfly) | | | | | |
| CC | **−0.89** | **−0.96** | **−0.70** | | | |
| | T300 (Butterfly) | | | T500 (Mixed) | | |
| CC | **−0.96** | **−0.97** | −0.62 | **−0.86** | **−0.86** | **−0.73** |
| | T700 (Horseshoe) | | | T850 (Horseshoe) | | |
| CC | −0.53 | −0.46 | **−0.74** | −0.55 | 0.03 | **−0.88** |

two downward branches are formed to the north and south of the Equator, and, as a result, the upper troposphere is warmed adiabatically. Similar processes occur with the opposite sign in the case of La Niña.

On the other hand, the horseshoe pattern is the direct response to the SST distribution of El Niño/La Niña. The pattern of SST warming, due to El Niño, ends up with the wide expansion of the warm water on the eastern side of the Pacific, which is produced by the coastal Kelvin waves along the North, and the South American continents.

Ting and Held (1990) and Barlow et al. (2002) applied the "perturbation model" of Nigam (1983) to the case of the simple dipole heating, and the heating in the eastern Equatorial Indian Ocean, respectively. The former captures the observed symmetry of the equatorial response, despite the gross asymmetry of the forcing. The latter calculates the stationary solution of 200 hPa stream-function over southeast Asia. However, the butterfly patterns, like Fig. 9, and the horseshoe patterns, like Fig. 10, are not reproduced by these simple models.

### *4.3 The polarity of signals over the Pacific and Indian sectors*

The degree of contrast between the El Niño and La Niña (shown in Figs. 9 and 10) is estimated with respect to three domains (see Fig. 5), namely domain I (South Asia; 231), domain II (Indonesia; 171), and domain III (Pacific; 1025), where the numbers in the parentheses are the total grid-points within the respective domains in the NCEP/NCAR reanalysis. The division of the three domains is made based on the concept of the Southern Oscillation, which consists of the South-Asian monsoon, El Niño/La Niña, and the updraft over the Maritime Continent.

Table 2 shows the correlation coefficients of MJJ temperature anomalies between El Niño and La Niña composite patterns. The cases are also separated using the index NINO3 SST in JAS. Table 2 and Figs. 9 and 10 complement each other for explaining the Southern Oscillation. Namely, Figs. 9 and 10 show the horizontal maps of the correlation only at two levels, i.e., 300 and 850 hPa. On the other hand, Table 2 provides the coefficients at various levels, i.e., 200, 300, 500, 700 and 850 hPa, but spatially in three domains, i.e., I, II and III.

This table indicates the remarkable polarity of air temperature associated with ENSO, particularly for $T_{300}$ in domain I and domain II. The correlation coefficients are −0.96 in domain I, and −0.97 in domain II. The $T_{850}$ in domain III also has high correlation, −0.88, and the $T_{500}$ has a correlation coefficient of −0.73. This supports the view that the SSTs for El Niño and La Niña are the cause for producing the horseshoe pattern. The symmetry with respect to ENSO for the three domains may be one of the important characteristics of the tropical-wide connection. Note that the low values at 700, and 850 hPa levels in domain I, are of no significance because these levels are underground.

Domain II corresponds to the Indonesian warm pool. The correlation coefficients in domain II for $T_{200}$ and $T_{300}$ (Table 2) are higher ($-0.97$ and $-0.96$) than those for $T_{500}$, $T_{700}$ and $T_{850}$ ($-0.86$, $-0.46$, and 0.03). It is worth noting that the correlation coefficient decreases with pressure, and it becomes almost zero at 850 hPa. This fact may be important, because it is related to the tropospheric biennial oscillation (TBO; see Barnett 1983; Yasunari 1987; Meehl 1987; Kiladis and van Loon 1988; Meehl 1993, 1997 and Meehl and Arblaster 2002a; among others). We shall return to the issue of the TBO.

Domain II was determined in the time-longitude diagrams by the correlation between the monsoon-related indices and SST. The ordinate of these diagrams (see Figs. 1–5 in Miyakoda et al. 1999) extends from year $-1$ to year $+1$ relative to the SA summer monsoon. The resulting patterns of correlation turn out to be divided into three regions for the abscissa. The central region is located between 100°E and 150°E, which corresponds to domain II.

Investigating the weak correlation in domain II, it is found that the separation between the positive and negative patterns is very much dependent on the host index; it is NINO3 SST (JAS) in Table 2. If the separation is done by another index, AIR (JJAS) or EASM (East Asian Summer Monsoon Index) (JJA), for example, a fairly different picture emerges. T850 in domain II will show a high value of negative correlation, between the positive and the negative ensemble means. This speculation is based on the results of Yasunari (1991) for AIR, and Shen and Lau (1995) for EASM. According to Tomita and Yasunari (1996), the SST variation around the Maritime Continent (roughly corresponds to domain II) has a TBO with "a phase transition that tends to occur about a half year earlier, that is, during the northern hemisphere autumn". In other words, the contrast of SST becomes stronger, if the two groups are separated by considering the phase of the TBO.

The existence of the substantial heat source in the area of the Indonesian Archipelago has been well known (see the cloud distribution in Fig. 3b of Klein et al. 1999). This area is also noted as the western tip of the outer rim of the horseshoe pattern, and it overlaps with the "tropical convective maximum" of 100°E–150°E (see Ju and Slingo 1995; Soman and Slingo 1997). Soman and Slingo (1997) find that the intensity of convection in the area of the tropical convective maximum is crucial for the SA-monsoon.

The TBO includes a two-year cycle, because of the seasonal locking of the summer monsoon, but the periodicity of IMR is, of course, not exactly two years. Meehl and Arblaster (2002b) state that "the TBO is not so much an oscillation, but a tendency for the system to flip-flop back and forth from year to year". It is very likely that this irregularity leads to a complication, referred to as the "spring predictability barrier". Another issue is that the intensity of IMR may or may not be affected by the QBO (Quasi-Biennial Oscillation in the stratosphere) (Parthasarathy and Mooley 1978; Bhalme and Jadhav 1984; Gray et al. 1992; Arpe et al. 1998). At any rate, the TBO is different from the QBO, in terms of its periodicity. On the other hand, the intensity of the variables related to TBO is known to be greatly influenced by ENSO.

## 5. Effect of ENSO on the SA-summer monsoon

### *5.1 Signals over the Tibetan Plateau and the updraft over the Indian subcontinent*

We now investigate how the signals in $H_{200-500}$ over the Tibetan Plateau, and $\omega 300$ over the Indian subcontinent, are produced by ENSO. An examination is made on the precursory character of ENSO signal in $H_{200-500}$, based on the correlation coefficients in Table 3. This paper treats the particular phase in which ENSO is the cause for the signals over the Tibetan Plateau and the upward motions over India. The numbers in the table should be looked at only above the main diagonal.

Before going further, an important point should be stressed. If the seasons of the two variables in a correlation are separated by "a spring", the values of the coefficient become unreasonably lower. This is referred to as the "spring predictability barrier". In this respect, however, the values on the diagonal in Table 3 are free from this barrier hazard. This table indicates that the maximum correlation in the upper right starts to increase in MAM or AMJ, implying that ENSO effects on the $H_{200-500}$ appear in the earlier part of the season. The im-

Table 3. Correlation between the H200–500 over the Tibetan Plateau and NINO3 SST for various seasons. The italic bold numbers are above 99.9% confidence level, and the bold numbers are between the 99.9% and 99.0% levels.

| | | H200–500 (Tibetan Plateau) | | | | | | |
|---|---|---|---|---|---|---|---|---|
| | | JFM | FMA | MAM | AMJ | MJJ | JJA | JAS |
| NINO3 | JFM | −0.01 | −0.02 | 0.00 | −0.10 | 0.03 | 0.20 | **0.38** |
| | FMA | −0.09 | −0.11 | −0.17 | −0.25 | −0.11 | 0.09 | 0.27 |
| | MAM | −0.19 | −0.24 | **−0.39** | **−0.41** | −0.27 | −0.04 | 0.11 |
| | AMJ | −0.26 | **−0.35** | ***−0.53*** | ***−0.51*** | **−0.35** | −0.10 | 0.03 |
| | MJJ | **−0.31** | **−0.44** | ***−0.64*** | ***−0.61*** | **−0.44** | −0.20 | −0.08 |
| | JJA | **−0.33** | ***−0.47*** | ***−0.67*** | ***−0.64*** | ***−0.47*** | −0.25 | −0.14 |
| | JAS | **−0.31** | **−0.46** | ***−0.60*** | ***−0.63*** | ***−0.48*** | −0.29 | −0.22 |

pacts of soil moisture and snow are not discussed in this paper (see Yang and Lau 1998 for a discussion of this aspect).

Table 4 shows the correlation between NINO3 SST and the first principal component of $\omega$300 over the smaller area of the Indian subcontinent, including a small portion of the Indian Ocean (see Fig. 5). In this case, the values should be above the diagonal, which are free from "the predictability barrier" hazard. Several features can be found from this table, together with Table 3. First, the correlation in Table 3 reaches the 99.0% confidence level in AMJ, and it remains high until MJJ. Second, the emergence of the monsoon characteristic of $\omega$300 (Table 4) appears slightly later (MJJ) than that in $H_{200-500}$ (Table 3). This is reasonable, because the seasonal heating over the Tibetan Plateau should come earlier than the land-sea contrast over the Indian sector due to the thermal inertia of the ocean. The reason for the existence of the precursory process was discussed in Staff members of Academia Sinica (1957); Luo and Yanai (1984); He et al. (1987); and Wu and Zhang (1998).

### 5.2 *La Niña-strong monsoon and El Niño-weak monsoon*

In order to demonstrate how the updraft over the Indian subcontinent is related to the SST over the Pacific and possibly the Indian Ocean, the geographical distribution of correlation between SST, and the first principal component of $\omega$300, is shown in Fig. 11. Note that the figure is only for the case of the smaller area of EOF analysis, and only for AMJ. The result for the larger area of EOF analysis indicates somewhat larger values of correlation than that for the smaller area of EOF analysis.

Figure 11 suggests the following. (a) The highest correlation region contributing to the updraft over India is the eastern equatorial Pacific, which includes the NINO3 region. (b) The correlation coefficients over the Arabian Sea are of opposite sign to those of the NINO3 region. (c) There is no high correlation value in the area of Indian Ocean dipole (see Ashok et al. 2001). Note that the period of the data is for 43 years, including before and after 1976 (see the later discussion in section 6). However, there are at least two caveats about this figure.

Table 4. Correlation between the first principal component (PC1) of $\omega$300 over the smaller area of the Indian subcontinent and NINO3 SST for various seasons. The italic bold numbers are above 99.9% conference level and the bold numbers are between the 99.9% and 99.0% levels.

| | | PC1 of $\omega$300 (Smaller Area) | | | | | | |
|---|---|---|---|---|---|---|---|---|
| | | JFM | FMA | MAM | AMJ | MJJ | JJA | JAS |
| NINO3 | JFM | 0.07 | −0.02 | 0.07 | −0.24 | −0.32 | −0.15 | 0 |
| | FMA | 0.01 | −0.12 | 0 | −0.37 | **−0.44** | −0.26 | −0.14 |
| | MAM | −0.11 | −0.24 | −0.15 | **−0.45** | ***−0.52*** | −0.34 | −0.25 |
| | AMJ | −0.19 | −0.31 | −0.26 | ***−0.50*** | ***−0.59*** | −0.37 | −0.29 |
| | MJJ | −0.22 | −0.31 | −0.27 | ***−0.49*** | ***−0.61*** | **−0.40** | −0.30 |
| | JJA | −0.18 | −0.26 | −0.24 | ***−0.49*** | ***−0.60*** | **−0.43** | −0.33 |
| | JAS | −0.11 | −0.19 | −0.19 | **−0.43** | ***−0.54*** | **−0.44** | −0.35 |

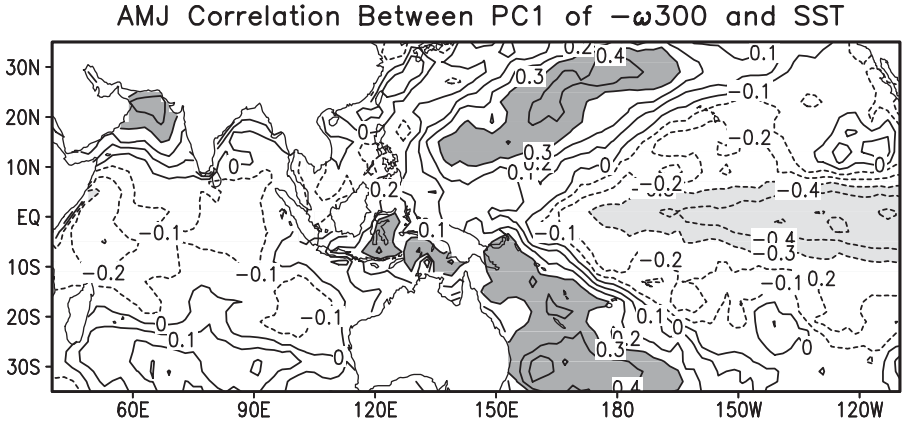


Fig. 11. Correlation between the first principal component of $-\omega$300 over the Indian subcontinent and grid-point SST (AMJ). Absolute values larger than 0.3 are shaded.

One is that the consideration of moisture is missing. Secondly, EOF mode 2, for example, is not taken into consideration.

The connection of the wind systems over the tropical Pacific and the Indian Oceans is investigated. Shown in Fig. 12 are composite patterns of AMJ wind anomaly at the 300 and 850 hPa levels. They are all constructed based on the same host index, NINO3 SST in AMJ. These wind fields correspond well to the temperature fields in Figs. 9 and 10. It can be seen that the cyclonic and anti-cyclonic circulation patterns co-locate with the positive and negative temperature anomalies, respectively, in the butterfly pattern. Several other points are worth noting. (1) Corresponding to the butterfly

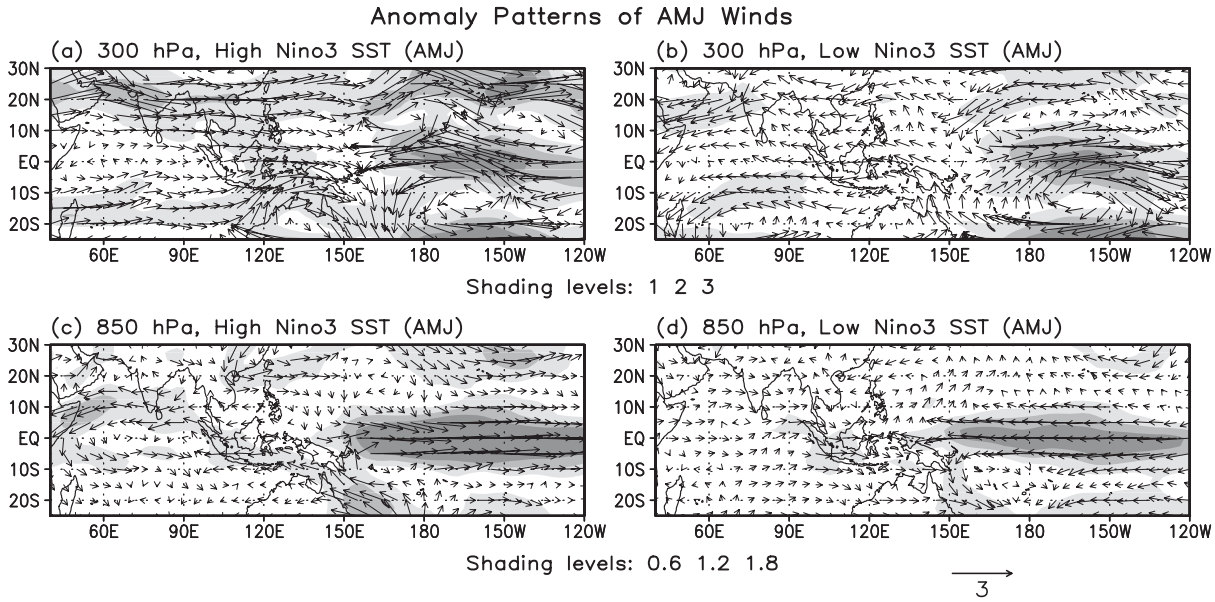


Fig. 12. Composite patterns of AMJ wind anomalies at 300 hPa (a and b) and 850 hPa (c and d). The cases are selected based on the AMJ NINO3 SST. The warm cases are 1957, 65, 69, 72, 82, 83, 87, 92, 93, and 97. The cold cases are 1955, 62, 64, 71, 73, 75, 78, 85, 88, and 96.

pattern at the 300 hPa level, there are anticyclonic (Fig. 12a) and cyclonic (Fig. 12b) anomalies at 20°N and 20°S, respectively, over the eastern Pacific. (2) Corresponding to the horseshoe pattern at the 850 hPa level, there are westerlies (Fig. 12c) and easterlies (Fig. 12d) in the anomaly flows, strongly concentrated near the Equator in the Pacific between 5°N and 5°S.

Similar to Fig. 12, Fig. 13 shows the composite patterns of AMJ wind anomaly at 300 and 850 hPa, but based on a different host index, i.e., H200–500 index (AMJ) over the Tibetan Plateau. This index is a measure of the premonsoon signal north of the Indian subcontinent (see the shaded area in Fig. 5). The polarity of the patterns between the high and low index cases (right and left) is clearer over the Indian sector than in Fig. 12, while the polarity is not so evident over the Pacific sector as in Fig. 12. Corresponding to the "lens" shape patterns at 300 hPa over the Tibetan Plateau, there are westerly anomaly (Fig. 13a) and easterly (Fig. 13b) flows at 15°–25°N. The 300 hPa flows over the Equator are quite zonal, and in opposite directions between over the Pacific sector, and over the Indian sector. At 850 hPa (Figs. 13c and 13d), the cross-equatorial wind is characteristic of the Somali Jet, which is always (summer and winter) directed northward in the mean. This kind of northward wind is found uniquely over the Indian Ocean (Li and Yanai 1996; Rodwell and Hoskins 2001). However, the anomalous components show a positive and negative alteration over the western Indian Ocean. The anomalous flow over the Bay of Bengal is counter-clockwise in Fig. 13c, and clockwise in Fig. 13d. These features are consistent with those shown by Kawamura (2000; see his Fig. 10) and Miyakoda et al. (2000).

There is, however, an apparent shortcoming in this method. Figure 12 provides an excellent representation of the flows for the Pacific longitudes (140°E–120°W) at both levels, but not for the Indian longitudes (40°–100°E). On the other hand, Fig. 13 is just the opposite, i.e., an excellent representation for the Indian longitudes, but not for the Pacific sector. A substantial effort was made in deriving suitable indices to represent the flow well simultaneously for both sectors (good for the Pacific sector as in Fig. 12, and good for the Indian sector as in Fig. 13 simultaneously). After testing many indices,

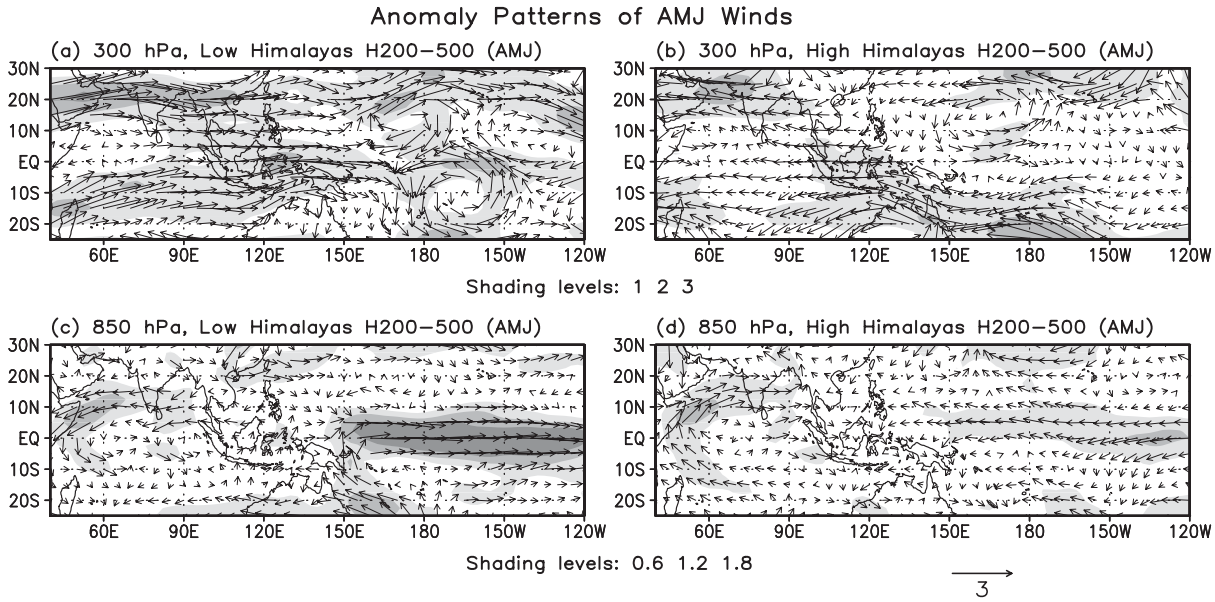


Fig. 13. Composite patterns of AMJ wind anomalies at 300 hPa (a and b) and 850 hPa (c and d). The cases are selected based on the AMJ thickness index (H200–500) over the Tibetan Plateau. The high H200–500 anomaly (AMJ) cases are 1957, 68, 72, 76, 77, 83, 87, 92, 93, and 97. The low H200–500 anomaly cases are 1956, 58, 61, 70, 73, 80, 84, 85, 88, and 90.

a single index has not been found that is capable of representing the variability over both oceans. Yet, the EOF analysis of the SST in the region 15°S–15°N, 150°W–90°W (the "broader NINO3" in Fig. 5) has an interesting property. The two leading modes can represent the two regions. The first mode (EOF 1) represents variability in the Pacific sector well, and the second mode (EOF 2) represents variability in the Indian sector well.

Lau and Nath (2000) used a general circulation model to investigate the concept of the atmospheric "bridging" related to the effect of ENSO on the Asian monsoon. They selected a small region, i.e., the tropical Pacific (25°S–25°N, 160°E–90°W), which may be called the "TOGA" region. The "TOGA" experiment was to run the GCM, specifying the observed SST in the TOGA region, and the climatological SST elsewhere in the world ocean. In contrast, the "GOGA" experiment was run with the same GCM, specifying the observed SST over the world oceans. They compared the simulation of the Indian summer monsoon rainfall obtained in the TOGA run with that of the GOGA run over the Indian subcontinent. Based on these experiments, they concluded that the rainfall in the two runs agree with each other fairly well, also agreeing with the observed rainfall. In other words, the SST in the tropical Pacific remotely affects the circulation, and the rainfall over the Indian sector, irrespective of the change in the local SST of the Indian Ocean.

In our case, however, the selected domain is even smaller than the TOGA region, i.e., "the broader NINO3 region (15°N–15°S, 150°W–90°W)". Besides the objective of the present study is different, i.e., this is an "index study" as opposed to a "GCM study". The pioneering work of an index study was by Pan and Oort (1983). They showed the spatial correlations between the monthly SST anomalies in the eastern Equatorial Pacific, and in other parts of the world ocean. They found that the SST in the eastern Equatorial Pacific over 20°S–20°N, and 180°–80°W, is very influential and, therefore, quite important. One of their conclusions is "that the SST anomalies in the tropical Indian and Atlantic Oceans lag behind those in the eastern Equatorial Pacific by, on average, 1 and 3 months, respectively".

To summarize the statistics of Figs. 6 and 7, Tables 3 and 4, and the EOF analysis above, a schematic diagram was constructed as shown

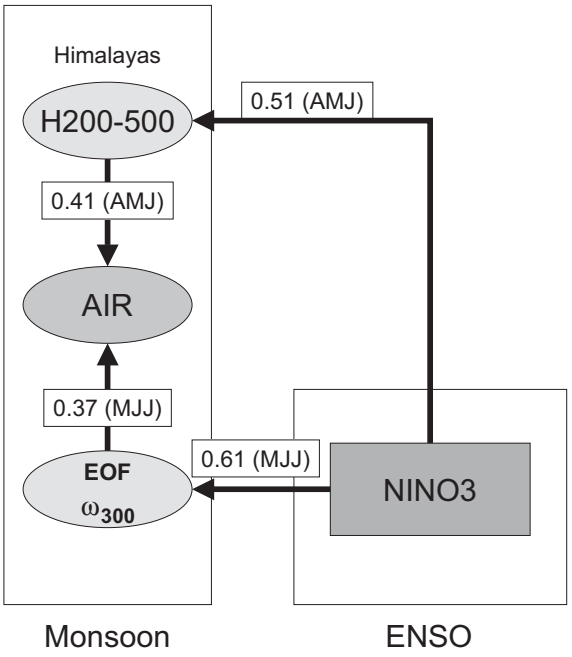


Fig. 14. Schematic diagram illustrating the connections among AIR, broader NINO3 SST, H200–500, and the first EOF mode of $\omega$300. The correlation coefficients are taken from Figs. 6 and 7 and Tables 3 and 4.

in Fig. 14. The figure indicates two interactive oscillation systems, ENSO and the SA-monsoon. Here, AIR is taken as an example for the illustration. In AMJ, NINO3 SST (AMJ) is significantly correlated with the precursory signal over the Tibetan Plateau, represented by $H_{200-500}$ (AMJ) ($R = 0.51$; see Table 3). In MJJ, NINO3 SST (MJJ) is strongly related with the updraft over the Indian subcontinent and the surrounding region, represented by the first EOF mode of $\omega$300 (MJJ) ($R = 0.61$; Table 4). These correlations suggest the appreciable contribution of both the $H_{200-500}$, and $\omega$300 to the subsequent summer monsoon, IMR ($R = 0.41$ and $R = 0.37$, respectively, not in tables).

Although the two arrows associated with the $H_{200-500}$ and $\omega$300 are directed toward the AIR, their contributions to the monsoon are different. One arrow is for the pre-monsoon period, and the other is for the main monsoon period. Of course, the diagram does not include all the processes associated with the monsoon. For example, the process in the layer between the ground surface and 500 hPa over the Tibetan Plateau is missing from the precursory signals (see Wu and Zhang 1998; Kawamura et al. 2001). In addition, the correlation coefficient between AIR and EOF 1 of $\omega$300 is only 0.37. This is too low; the effect of EOF 2 of $\omega$300 should also be taken into account. Besides, $\omega$300 alone cannot explain the total monsoon rainfall and other factors like moisture supply should be considered. Another question is what is the role played by domain II, i.e., the Maritime Continent.

## 6. Climate change circa 1976

### *6.1 The outline for the process from the ENSO to monsoon*

Table 5 shows the correlation between various monsoon indices, and the $H_{200-500}$ (MAM) over the Tibetan Plateau (the third column), as well as the first principal component (PC1) of $\omega$300 (AMJ) over the Indian subcontinent (the fourth column). First, the third column of this table (H200–500 (MAM)) indicates that no significant difference can be found for all indices, except AIR, in the precursory signals between the period before, and after, 1976. Secondly, the fourth column of Table 5 (PC1 of $\omega$300) indicates no significant difference in the vertical motion over the area surrounding India between the period before, and after, 1976 for AIR, while a slight difference is apparent in W-Y and MTG. This difference might be relevant to the SST over the Indian Ocean, as will be discussed later.

The correlation between NINO3 SST of AMJ and JAS (of year 0) is shown in Table 6, and the monsoon indices for JAS (+1 year), including MHI (the Monsoon Hadley Circulation Index). First, the third column of Table 6 (AMJ) indicates that no significant difference can be found for all indices, except AIR, between the periods before, and after, 1976. Secondly, the fourth column of Table 6 (JAS) also indicates the same character.

### *6.2 Hypothesis on the climate change circa 1976*

There are a number of papers which report the rather sudden change of global climate circa 1976. For example, Folland and Parker (1995; global SST), Federov and Philander (2001; SST over the equatorial Pacific), and

Table 5. Correlation of H200–500 and PC1 of $\omega$300 with various monsoon indices, for the periods 1955–75 and 1976–97. The italic bold numbers are above 99.9% confidence level, and the bold numbers are between the 99.9% and 90.0% levels.

| | | H200–500 (MAM) | PC1 of $\omega$300 (AMJ) |
|---|---|---|---|
| AIR | 1955–75 | ***0.73*** | **0.43** |
| | 1976–97 | 0.19 | 0.32 |
| W-Y | 1955–75 | **0.43** | 0.35 |
| | 1976–97 | **0.63** | **0.67** |
| MTG | 1955–75 | **0.53** | **0.4** |
| | 1976–97 | **0.63** | **0.67** |

Table 6. Correlation between the monsoon indices and Nino3 SST in two seasons (AMJ and JAS) for the periods 1955–75 and 1976–97. Note that the monsoon Hadley Circulation index (MHI) is added.

| | | NINO3 SST | |
|---|---|---|---|
| | | AMJ | JAS |
| AIR | 1955–75 | **−0.45** | ***−0.74*** |
| | 1976–97 | −0.16 | −0.25 |
| W-Y | 1955–75 | **−0.43** | **−0.61** |
| | 1976–97 | **−0.54** | **−0.57** |
| MTG | 1955–75 | **−0.63** | ***−0.73*** |
| | 1976–97 | ***−0.75*** | **−0.68** |
| MHI | 1955–75 | **−0.63** | ***−0.76*** |
| | 1976–97 | ***−0.75*** | **−0.63** |

Mantua et al. (1997; salmon catch in the northern Pacific) have all commented on the abrupt change of climate regime circa 1976, explicitly or implicitly. Also, the Caspian Sea level dropped from 1940 to 1976, and then suddenly started to rise in 1977 (L. Bengtsson and K. Arpe, personal communication).

Based on these findings, one can hypothesize that the year 1976 was the turning point of the climate change. The scenario relevant to the present discussion goes as follows. Associated with global climate change, the atmospheric temperature in the lower level is increased in some regions. For example, the lower atmosphere in Siberia tends to have clockwise circulation anomalies centered over a region south of Lake Baikal (see Figs. 6 and 7 of Kinter et al. 2002). This cyclonic anomaly creates strong westerlies to its south that extend eastward at 35°–50°N over the Kuroshio extension of the Pacific Ocean. The anomalous westerlies have an anomalous wind curl that is responsible for creating the anomalously cold SST in the central Pacific (see Yasuda and Hanawa 1997; Deser et al. 1999, for example).

Anomalous northerlies form between the Siberian low and the north Pacific high. Within the period 1955–1997, anomalous southward flow (denoted $V_{ch}$ in Kinter et al. 2002) is only found after 1976. The circulation anomaly in the lower atmosphere is also associated with a westerly anomaly (denoted $U_{ph}$ in Kinter et al.) east of the Philippines, which reinforces the monsoon westerlies. The enhanced westerly anomalies show up in the stronger, or more frequent, westerly wind bursts in that region.

The westerly bursts, represented by $U_{ph}$, are crucial for the ENSO initiation. Before 1976, $U_{ph}$ was associated mainly with the SA-monsoon, while after 1976, $U_{ph}$ was affected by both the monsoon and $V_{ch}$. Consequently, the connection between the monsoon and ENSO became substantially weaker after 1976. In particular, the lag correlation between the summer monsoon of JJA (year 0), or JJAS (year 0) and

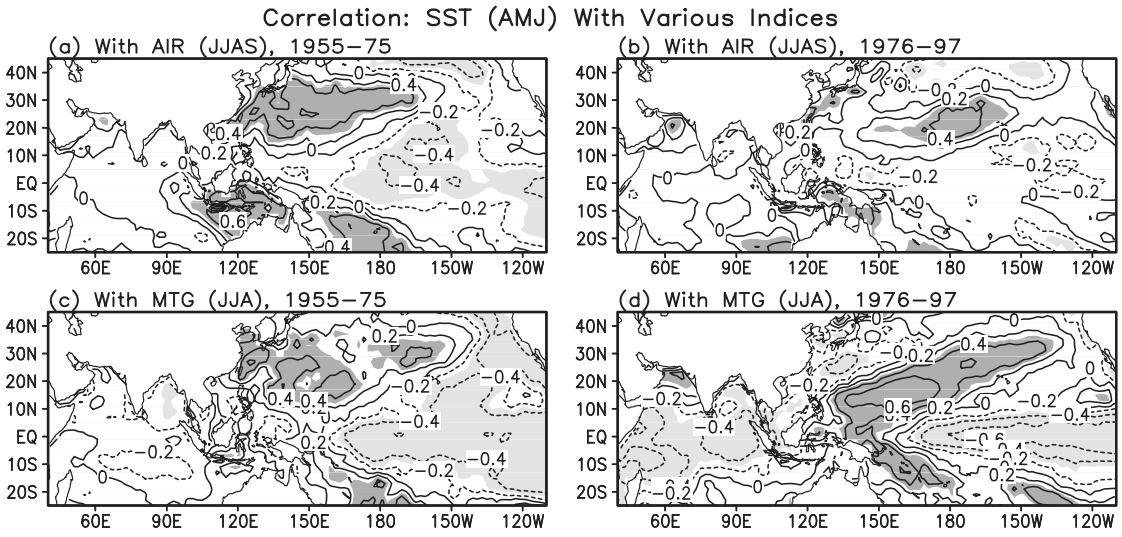


Fig. 15. Correlation between the AIR and grid-point SST (AMJ) for the periods 1955–75 (a) and 1976–97 (b). Shown also is the correlation between MTG and the AMJ SST (c and d). Absolute values larger than 0.3 are shaded.

NINO3 SST (NDJ) changed, before and after 1976, from −0.66 to −0.33 for AIR; from −0.59 to −0.28 for W-Y, from −0.73 to −0.42 for MTG, and from −0.55 to −0.16 for MHI (see Miyakoda et al. 2000 and Kinter et al. 2002), where the summer monsoon implies JJAS for AIR, and JAS for other monsoon indices.

The foregoing argument leads to the explanation why the monsoon-to-ENSO process changed circa 1976, but the ENSO-to-monsoon process remained unchanged (except in the case of AIR). In the process from the SA-monsoon to ENSO, the atmospheric teleconnection is confined to the lower levels. In particular, the crucial area is the western part of the tropical Pacific, e.g., east of the Philippine Islands. On the other hand, in the reverse process, i.e., from ENSO to the monsoon, the teleconnection takes place through the whole atmosphere, i.e., in terms of the butterfly pattern and the horseshoe pattern. Therefore, the existence of cold water over the North Pacific does not seriously affect the westward teleconnection.

### *6.3 The effect of the Indian Ocean on the SA-monsoon*

A slightly different view has recently emerged. The Indian Ocean SST has been significantly correlated with AIR after 1976, but not before 1976 (Harzallah and Sadourny 1997; Clark et al. 2000; Ashok et al. 2001). In particular, in the case of the 1998 monsoon, the influence of the Indian Ocean cannot be ignored (Ueda and Matsumoto 2000; Shen et al. 2001; Schubert and Wu 2001).

Ashok et al. (2001) argued further that "the Indian Ocean Dipole (IOD) and ENSO have complementarily affected the AIR during the last four decades", and that "whenever the ENSO-AIR correlation is low (high), the IOD-AIR correlation is high (low)".

In order to describe this relationship in the context of our index study, Fig. 15 is shown. It is seen from this figure that, for the period 1976–1997, the most organized shape is in the case of MTG (Fig. 15d), and the least organized shape is in the case of AIR (Fig. 15b). The figure clearly confirms what is implied by the third column (AMJ) of Table 6.

Figure 15 also shows that, compared with AIR, MTG is associated with a much more prominent and extensive feature over the Pacific and Indian Oceans. This may be partly due to the size of the areas that are used for defining the indices. The MTG is based on the information of a broad domain, while the AIR represents the rainfall confined to a much smaller area. In addition, a comparison of the domains for AIR and MHI leads to the speculation that

the Burmese mountains may be a substantial obstacle for the teleconnection between India and the eastern Pacific (Hahn and Manabe 1975). Besides, moisture is an important factor for consideration of AIR. The contribution of moisture, has not been investigated.

As described earlier, the weaker connection from the SA-monsoon to ENSO during 1976–1997 is ascribed to the surface wind shift, and hence, the colder water in the north Pacific. To examine the impact of the cold water on the reverse process, from ENSO to the monsoon, the cold SST anomalies are subtracted (removed) from the total SST in the period 1976–97, and reproduce a figure similar to Fig. 15 using the artificially-constructed SST. The result obtained (not shown) is similar to that shown in Fig. 15, indicating that the emergence of the cold water has little effect on the connection from ENSO to the monsoon.

## 7. Conclusions and comments

Two of the most dominant large-scale phenomena of the atmosphere, and the ocean, are El Niño/La Niña (or ENSO) and the South Asian summer monsoon. This paper addresses the process from ENSO to the South Asian monsoon, without discussing the individual processes within each phenomenon.

A pre-monsoon signal in the 200–500 hPa thickness over the Tibetan Plateau is apparent in March-April-May-June, consistent with the results of Kawamura (1998) and Liu and Yanai (2001). It is emphasized that this precursory signal is dispatched from the tropical and mid-latitude Pacific area associated with ENSO, and enhanced at the Tibetan Plateau. The signal in the thickness, $H_{200-500}$, is originally generated in January-February-March or earlier in the Pacific area, and emanates westward in the mid-latitudes. It then propagates westward in the latitude belt 20°–35°N. The zonal movement from Asia, via the Tibetan Plateau to the Atlantic Ocean and back, may be associated with the seasonal migration of the heated area.

In addition, the monsoon upward motions over the Indian subcontinent and its surrounding area are evoked by the local seasonal heating (internal), but their anomalies are mostly controlled by ENSO (external). The extent of the ENSO impact on the monsoon is seen in the vertical motion at 300 hPa level over the Indian area. The correlation between NINO3 SST, and the first EOF mode of the vertical motion, reaches its maximum in April-May-June (correlation $R = 0.50$, Fig. 7), and in May-June-July ($R = 0.61$). However, the maximum of the rainfall appears later in July-August-September from the view of AIR ($R = 0.64$, Fig. 7). The reason for the delay would be that the rainfall is contributed not only by the vertical velocity, but also by the supply of water vapor.

The ENSO signal propagates westward from the eastern Pacific to the Indian longitudes through various atmospheric variables. This propagation takes place in conjunction with the butterfly pattern in the upper troposphere above 500 hPa, and with the horseshoe pattern in the lower troposphere below 500 hPa, both in the central and eastern Pacific.

The butterfly pattern is the manifestation of the emanation of the ENSO signal from the central and eastern tropical Pacific toward the Indian longitudes, which is the extended mode of heating discussed by the Matsuno (1966) and Gill (1980) type dynamics. On the other hand, the horseshoe pattern is the direct response to the SST distribution of El Niño. In addition, the heating over the Maritime Continent may be very important for the formation of the tropical circulation system over the Indian sector. However, this heating may be also controlled by ENSO. In order to confirm this speculation, and to understand the mechanism and their role in ENSO and the SA-monsoon, a study is needed along the line of the perturbation model or the anomaly model described in section 4, including the consideration of water vapor.

The EOF analysis of the SST in "the broader NINO3 region (15°N–15°S, 150°W–90°W)" reveals an interesting property. The two leading modes of the EOF analysis represent fairly well the fields of horizontal wind vectors, and temperature for the Pacific sector (the first mode) and the Indian sector (between about 30°N and 30°S) (the second mode) in terms of regression. It is found that the SST in the NINO3 region is the most dominant heat source for the tropical Pacific as well as the Indian sector. This is an extended view of Pan and Oort (1983).

The correlation between the NINO3 SST and various monsoon indices is reasonably high before and after 1976, except for the low correla-

tion between AIR and SST. This fact suggests that the long-term variability of the process from ENSO to the monsoon is almost the same throughout the whole period (except IMR). Therefore, this feature is quite different from that of the reverse process, as shown by Miyakoda et al. (2000) and Kinter et al. (2002). Namely, the intensity of the SA-summer monsoon is a good precursor for the ENSO of the subsequent winter before 1976, but this relationship has partially broken down after 1976.

A possible explanation is as follows. In the process from the monsoon to ENSO, the atmospheric teleconnection is confined to the lower levels, while in the process from ENSO to the monsoon (discussed in this paper), the teleconnection takes place throughout the whole troposphere, i.e., 850 hPa∼200 hPa at least in the forms of the horseshoe and the butterfly patterns.

It is remarked, however, that the monsoon index, AIR, behaves somewhat differently from other monsoon indices for the South-Asian monsoon. There are several factors that should be taken into consideration. One factor is that AIR is based on the precipitation, while other indices are not. This means that the moisture may be an important factor. A second factor is that, as Matsumoto and Murakami (2002) have shown, the SA-monsoon is not well defined. The rainfall over the Bay of Bengal belongs to the "Southeast Asian Monsoon", while the rainfall over the Indian subcontinent may belong to a different system. A third factor is that, as Ashok et al. (2001) pointed out, AIR might be affected by the "Indian Ocean Dipole".

## Acknowledgements

We are grateful to Prof. J. Shukla and Dr. K. Mooney for arranging for K. Miyakoda to work at George Mason University and COLA. Several scientists including M. Fennessy, V. Misra, B. Huang, B. Kirtman, A. Schlosser and E. Schneider have kindly contributed to this work. The authors would like to thank Profs. R. Kawamura, M. Yanai, R. Stouffer, Dr. K. Arpe, and Prof. Ueda, the editor of the Journal of Meteorological Society of Japan.

## References

Angel, J.K., 1981: Comparison of variation in atmospheric quantities with sea surface temperature variations in the equatorial eastern Pacific. *Mon. Wea. Rev.*, **109**, 230–243.

Arpe, K.L., L. Dumenil, and M.A. Giorgetta, 1998: Variability of the Indian monsoon in the ECHAM 3 model: sensitivity to sea surface temperature, soil moisture, and the stratospheric quasi-biennial oscillation. *J. Climate*, **11**, 1837–1958.

Ashok, K., Z. Guan, and T. Yamagata, 2001: Impact of the Indian Ocean dipole on the relationship between the Indian monsoon rainfall and ENSO. *Geophys. Res. Let.*, **28**, 4499–4502.

Barlow, M., H. Cullen, and B. Lyon, 2002: Drought in central and southwest Asia: La Niña, the warm pool, and Indian Ocean precipitation. *J. Climate*, **15**, 697–700.

Barnett, T.P., 1983: Interaction of the monsoon and Pacific trade wind system at interannual time scales. Part I: The Equatorial zone. *Mon. Wea. Rev.*, **111**, 756–775.

Bhalme, H.N. and S.K. Jadhav, 1984: The Southern Oscillation and its relation to the monsoon rainfall. *J. Climatol.*, **4**, 509–520.

Brankovic, C., T.N. Palmer, and L. Ferranti, 1994: Predictability of seasonal atmospheric variation. *J. Climate*, **7**, 217–237.

Chandrasekar, A. and A. Kitoh, 1998: Impact of localized sea surface temperature anomalies over the equatorial Indian Ocean on the Indian summer monsoon. *J. Meteor. Soc. Japan*, **76**, 841–853.

Clark, C.O., J.E. Cole, and P.J. Webster, 2000: Indian Ocean SST and Indian Summer rainfall: Predictive relationship and their decadal variability. *J. Climate*, **13**, 2503–2519.

Deser, C., M.A. Alexander, and M.S. Timlin, 1999: Evidence for a wind-driven intensification of the Kuroshio current extension from the 1970s to the 1980s. *J. Climate*, **12**, 1697–1706.

Fedorov, A.V. and S.G. Philander, 2001: A stability analysis of tropical ocean-atmosphere interactions: bridging measurements and theory for El Niño. *J. Climate*, **14**, 3086–3101.

Flohn, H. 1957: Large-scale aspects of the "summer monsoon" in South and East Asia. *J. Meteor. Soc. Japan*, 75th Ann. Vol., 180–186.

Folland, C.K. and D.E. Parker, 1995: Correction of instrumental biases in historical sea surface temperature data. *Quart. J. Roy. Meteor. Soc.*, **121**, 319–369.

Gill, A.E. 1980: Some simple solutions for heat-induced tropical circulation. *Quart. J. Roy. Meteor. Soc.*, **106**, 447–462.

Goswami, B.N., V. Krishnamurthy, and H. Annamalai, 1999: A broad scale circulation index for interannual variability of the Indian summer

monsoon. *Quart. J. Roy. Meteor. Soc.*, **125**, 611–633.

Gray, W.M., J.D. Sheaffer, and J.A. Knaff, 1992: Influence of the stratospheric QBO on ENSO variability. *J. Meteor. Soc. Japan*, **70**, 975–995.

Hahn, D.G. and S. Manabe, 1975: The role of mountains in the South Asian monsoon circulation. *J. Atmos. Sci.*, **32**, 1515–1541.

Harzallah, R. and R. Sadourny, 1997: Observed lead-lag relationships between Indian summer monsoon and some meteorological variables. *Clim. Dyn.*, **13**, 635–648.

He, H., J.W. McGinnis, Z. Song, and M. Yanai, 1987: Onset of the Asian monsoon in 1979 and the effect of the Tibetan Plateau. *Mon. Wea. Rev.*, **115**, 1966–1995.

Ju, J. and J.M. Slingo, 1995: The Asian summer monsoon and ENSO. *Quart. J. Roy Meteor. Soc.*, **121**, 1133–1162.

Kalnay, E. and Coauthors, 1996: The NCEP/NCAR 40-year reanalysis project. *Bull. Amer. Meteor. Soc.*, **77**, 437–472.

Kawamura, R., 1998: A possible mechanism of the Asian summer monsoon-ENSO coupling. *J. Meteor. Soc. Japan*, **76**, 1009–1027.

———, 2000: The Asian summer monsoon-ENSO coupling-Toward understanding of atmosphere-ocean interaction in the Indian Ocean. (in Japanese). *Tenki*, **47**, 169–181.

———, T. Matsuura, and S. Iizuka, 2001: Role of equatorially asymmetric sea surface temperature anomalies in the Indian Ocean in the Asian summer monsoon and El Niño-Southern Oscillation coupling. *J. Geophy. Res.*, **106**, 4681–4693.

Kiladis, G.N. and H. van Loon, 1988: The Southern Oscillation. Part VII: Meteorological anomalies over the Indian and Pacific sectors associated with the extremes of the oscillation. *Mon. Wea. Rev.*, **116**, 120–136.

Kinter, III J.L., K. Miyakoda, and S. Yang, 2002: Recent change in the connection from the Asian monsoon to ENSO. *J. Climate*, **15**, 1203–1215.

Klein, S.A., B.J. Soden, and N.-C. Lau, 1999: Remote sea surface temperature variations during ENSO: evidence for a tropical atmospheric bridge. *J. Climate*, **12**, 917–932.

Lau, K.-M., K.-M. Kim, and S. Yang, 2000: Dynamical and boundary forcing characteristics of regional components of the Asian summer monsoon. *J. Climate*, **13**, 2461–2482.

Lau, N.-C. and M.J. Nath, 2000: Impact of ENSO on the variability of the Asian-Australian monsoons as simulated in GCM experiments. *J. Climate*, **13**, 4287–4309.

Li, C. and M. Yanai, 1996: The onset and interannual variability of the Asian summer monsoon in relation to land-sea thermal contrast. *J. Climate*, **9**, 358–375.

Liu, C. and M. Yanai, 2001: Relationship between the Indian monsoon rainfall and the tropospheric temperature over the Eurasian continent. *Quart. J. Roy. Meteor. Soc.*, **127**, 909–937.

Luo, H. and M. Yanai, 1984: The large-scale circulation and heat sources over the Tibetan Plateau and surrounding areas during the early summer of 1979. Part II: Heat and moisture budget. *Mon. Wea. Rev.*, **112**, 966–989.

Mantua, J.N., S.R. Hare, Y. Zhang, J.M. Wallace, and R.C. Francis, 1997: A Pacific interdecadal climate oscillation with impacts on salmon production. *Bull. Amer. Meteor. Soc.*, **78**, 1069–1080.

Matsumoto, J. and T. Murakami, 2002: Seasonal migration of monsoons between the northern and southern hemisphere as revealed from equatorially symmetric and asymmetric OLR data. *J. Meteor. Soc. Japan*, **80**, 419–437.

Matsuno, T., 1966: Quasi-geostrophic motions in the equatorial area. *J. Meteor. Soc. Japan*, **44**, 25–43.

Meehl, G.A., 1987: The annual cycle and interannual variability in the tropical Indian and Pacific Ocean regions. *Mon. Wea. Rev.*, **115**, 27–50.

———, 1993: A coupled air-sea biennial mechanism in the tropical Indian and Pacific regions: Role of the ocean. *J. Climate*, **6**, 31–41.

———, 1997: The south Asian monsoon and the tropospheric biennial oscillation. *J. Climate*, **10**, 1921–1943.

——— and J.M. Arblaster, 2002a: The tropospheric biennial oscillation and Asian-Australian monsoon rainfall. *J. Climate*, **15**, 722–744.

——— and ———, 2002b: GCM sensitivity experiments for the Indian monsoon and tropospheric biennial oscillation transition conditions. *J. Climate*, **15**, 923–944.

Miyakoda, K., A. Navarra, and M.N. Ward, 1999: Tropical-wide teleconnection. II: The ENSO-monsoon system. *Quart. J. Roy. Meteor. Soc.*, **125**, 2937–2963.

———, J.L. Kinter III, and S. Yang, 2000: Analysis of the connection from the South Asian monsoons to ENSO by using precipitation and circulation indices. *COLA Tech. Rep.*, **90**, 72p.

Mooley, D.A. and B. Parthasarathy, 1983: Variability of the Indian summer monsoon and tropical circulation feature. *Mon. Wea. Rev.*, **111**, 967–978.

Navarra, A. and K. Miyakoda, 1988: Anomaly general circulation models. *J. Atmos. Sci.*, **45**, 1509–1530.

———, M.N. Ward, and K. Miyakoda, 1999: Tropical-wide teleconnection and oscillation. I: Teleconnection indices and type I/II states. *Quart. J. Roy. Meteor. Soc.*, **125**, 2909–2935.

Nigam, S., 1983: *On the structure and forcing of tropospheric stationary waves*. PhD. thesis, Princeton University, Princeton, NJ 08544, pp203.

———, I. Held, and S. Lyons, 1986: Linear simulations of the stationary eddies in a GCM. Part I: The "no-mountain" model. *J. Atmos. Sci.*, **43**, 2944–2961.

———, I. Held, and S. Lyons, 1988: Linear simulations of the stationary eddies in a GCM. Part II: The "mountain" model. *J. Atmos. Sci.*, **45**, 1433–1452.

Palmer, T.N., C. Brankovic, P. Viterbo, and M.J. Miller, 1992: Modelling interannual variations of summer monsoons. *J. Climate*, **5**, 399–417.

Pan, Y.-H. and A.H. Oort, 1983: Global climate variations connected with sea surface temperature anomalies in the eastern equatorial Pacific for the 1958–73 period. *Mon. Wea. Rev.*, **111**, 1244–1258.

Parthasarathy, B. and D.A. Mooley, 1978: Some feature of a long homogeneous series of Indian summer monsoon rainfall. *Mon. Wea. Rev.*, **106**, 771–781.

Rasmusson, E.M. and T.H. Carpenter, 1983: The relationship between the eastern Pacific sea surface temperature and rainfall over India and Sri Lanka. *Mon. Wea. Rev.*, **111**, 354–384.

Reynolds, R.W. and T.M. Smith, 1994: Improved global sea surface temperature analysis using optimum interpolation. *J. Climate*, **7**, 929–948.

Rodwell, M.J. and B.J. Hoskins, 2001: Subtropical anticyclones and summer monsoons. *J. Climate*, **14**, 3192–3211.

Ropelewski, C.F. and M.S. Halpert, 1989: Global and regional scale precipitation patterns associated with the El Niño/Southern Oscillation. *Mon. Wea. Rev.*, **115**, 1606–1626.

Saji, N.H., B.N. Goswami, P.N. Vinayachandran, and T. Yamagata, 1999: A dipole made in the tropical Indian Ocean. *Nature*, **401**, 360–363.

Schubert, S.D. and M.-L. Wu, 2001: Predictability of the 1997 and 1998 South Asian summer monsoon low-level winds. *J. Climate*, **14**, 3173–3191.

Shen, S. and K.-M. Lau, 1995: Biennial oscillation associated with the East Asian summer monsoon and tropical sea surface temperature. *J. Meteor. Soc. Japan*, **73**, 105–124.

Shen, X. and M. Kimoto, 1999: Influence of El Niño on the 1997 Indian summer monsoon. *J. Meteor. Soc. Japan*, **77**, 1023–1037.

———, ———, H. Kimoto, A. Sumi, A. Numaguchi, and J. Matsumoto, 2001: Simulation of the 1998 East Asian summer monsoon by CCSR/NIES AGCM. *J. Meteor. Soc. Japan*, **79**, 741–757.

Shukla, J. 1975: Effects of Arabian sea surface temperature anomaly on Indian summer monsoon: A numerical experiment with the GFDL model. *J. Atmos. Sci.*, **32**, 503–511.

——— and D.A. Paolino, 1983: The southern oscillation and long range forecasting of the summer monsoon rainfall over India. *Mon. Wea. Rev.*, **111**, 1830–1837.

Soman, M.K. and J.M. Slingo, 1997: Sensitivity of the Asian summer monsoon to aspects of sea-surface-temperature anomalies in the tropical Pacific Ocean. *Quart. J. Roy. Meteor. Soc.*, **123**, 309–336.

Staff Members of the Academia Sinica, 1957: On the general circulation over eastern Asia. *Tellus*, **9**, 432–446.

Ting, M. and I.M. Held, 1990: The stationary wave response to a tropical SST anomaly in an idealized GCM. *J. Atmos. Sci.*, **47**, 2546–2566.

Tomita, T. and Y. Yasunari, 1996: Role of the northeast winter monsoon on the biennial oscillation of the ENSO/Monsoon system. *J. Meteor. Soc. Japan*, **74**, 399–413.

Ueda, H. and J. Matsumoto, 2000: A possible triggering process of east-west asymmetric anomalies over the Indian Ocean in relation to 1997/98 El Niño. *J. Meteor. Soc. Japan*, **78**, 803–818.

Wang, B., R. Wu, and X. Fu, 2000: Pacific-East Asian teleconnection: How does ENSO affect East Asian climate? *J. Climate*, **13**, 1517–1536.

Washington, W.M., R.M. Chervin, and G.V. Rao, 1977: Effects of a variety of Indian Ocean surface temperature anomaly patterns on the summer monsoon circulation: Experiments with the NCAR general circulation model. *Pageoph*, **115**, 1335–1356.

Webster, P.J. and S. Yang, 1992: Monsoon and ENSO: Selectively interactive systems. *Quart. J. Roy. Meteor. Soc.*, **118**, 877–926.

——— and Co-authors, 1998: Monsoon processes, predictability, and the prospects of prediction. *J. Geophys. Res.*, **103**, 14,451–14,510.

Wu, G. and Y. Zhang, 1998: Tibetan Plateau forcing and the timing of the monsoon onset over the South Asia and the South China Sea. *Mon. Wea. Rev.*, **126**, 913–927.

Yamazaki, K., 1988: Influence of sea surface temperature anomalies over the Indian Ocean and Pacific Ocean on the tropical atmospheric circulation: A numerical experiment. *J. Meteor. Soc. Japan*, **66**, 797–806.

Yanai, M., C. Li, and Z. Song, 1992: Seasonal heating of the Tibetan Plateau and its effects on the

evolution of the Asian summer monsoon. *J. Meteor. Soc. Japan*, **70**, 319–351.

Yang, S. and K.-M. Lau, 1998: Influence of SST and ground wetness anomalies on the Asian summer monsoon. *J. Climate*, **11**, 3320–3246.

———, K.-M. Lau, and M. Sanka-Rao, 1996: Precursory signals associated with the interannual variability of the Asian summer monsoon. *J. Climate*, **9**, 949–964.

Yasuda, T. and K. Hanawa, 1997: Decadal changes in the mode waters in the midlatitude North Pacific. *J. Phys. Oceanogr.*, **27**, 858–870.

Yasunari, T., 1987: Global structure of the El Niño/Southern Oscillation. Part II: Time evolution. *J. Meteor. Soc. Japan*, **65**, 81–102.

———, 1991: "The monsoon year"—A new concept of the climatic years in the tropics. *Bull. Amer. Meteor. Soc.*, **72**, 1331–1338.